Bulletin of the Seismological Society of America, Vol. 109, No. 2, pp. 756–769, April 2019, doi: 10.1785/0120180167

Surface Deformations and Rupture Processes Associated with the 2017 M_w 5.4 Pohang, Korea, Earthquake

by Jin-Hyuck Choi, Kyoungtae Ko, Yong Sik Gihm, Chang Soo Cho, Hoonyol Lee, Seok Goo Song, Eun-Seok Bang, Hong-Jin Lee, Han-Kyung Bae, Sung Won Kim, Sung-Ja Choi, Sung Soon Lee, and Seung Ryeol Lee

Abstract In November 2017, an M_w 5.4 earthquake with a shallow (~4 km) hypocenter occurred in the Pohang area, one of the most developing industrial cities in South Korea. This shock resulted in the costliest earthquake damages in modern Korean history. Immediately after the event, it was not easy to recognize the source fault due to the lack of clear coseismic surface ruptures but also the absence of previously mapped active faults around the epicenter. Based on satellite- and unmanned aerial vehicle (UAV)-derived images, with ground resolution higher than 0.5 m, and field observations, we investigate surface deformation such as sand blows and ground failures associated with the Pohang earthquake as well as bedrock fault exposures in the epicentral area. To better constrain the source fault and deformation mechanism, we combine both moment tensors with aftershock relocations and surface displacements estimated by Interferometric Synthetic Aperture Radar (InSAR). Our results indicate that (1) various types and distributions of secondary ground deformation were controlled by blind oblique-slip rupture; characterized by right-lateral and reverse-slip components, on a reactivated pre-existing segmented normal-fault system, and (2) local ground conditions could trigger or amplify ground deformations and their related earthquake damage. Our study highlights the importance of mapping the extent of coseismic deformation as well as the trace of active faults on improving seismic hazard assessments in the Korean Peninsula.

Introduction

An M_w 5.4 earthquake hits the city of Pohang, a major industrial area in South Korea, at 14:29:32 KST on 15 November 2017. The hypocenter of this earthquake was at about 4 km depth and 10 km east of the Yangsan fault, which is the closest mapped neotectonically active major fault near the epicenter (Lee and Na, 1983; Kyung, 2003). This event ranks second in magnitude behind the 14 km deep September 2016 M_w 5.5 Gyeongju earthquake in instrumental history in South Korea. Yet, extensive damage to facilities, about six times as large as that of the 2016 Gyeongju earthquake, occurred during the 2017 Pohang earthquake. The earthquake was close (< 1 km) to a fluid-injection well associated with the enhanced geothermal systems, and hence raised questions of the possibility of induced seismicity (Grigoli *et al.*, 2018; Kim *et al.*, 2018). Despite the shallow hypocenter, coseismic surface rupture was not observed; however, a variety of secondary ground deformation such as sand blows and ground cracks was widely distributed around the epicentral area.

In general, surface ruptures are associated with large earthquakes with magnitudes greater than ~6.5 and sometimes occur during shallow moderate-sized earthquakes. Modern remote sensing techniques such as Interferometric Synthetic Aperture Radar (InSAR) and satellite imagery analyses allow for the rapid recognition of surface ruptures and offset determination immediately following an earthquake, and can guide detailed field investigation. Remote sensing and field results, together with seismological records, can provide details on the source geometry of the earthquake and characteristics of coseismic rupture processes (Champenois *et al.*, 2017; Grandin *et al.*, 2017). These data contribute to short-term earthquake response assessments and help define sites for further paleoseismological studies (long-term seismic hazard assessments). In some cases, earthquakes large enough to cause destructive damage do not generate surface ruptures (Talebian *et al.*, 2004; Ainscoe *et al.*, 2017; Lekkas *et al.*, 2018). This has been the case for several historical earthquakes including large earthquakes on low-angle fault systems and moderate-sized earthquakes in urban areas (e.g., the 1994 Northridge, California; the 2003 Bam, Iran; and the 2015 Gorkha, Nepal, earthquakes). The lack of surface

rupture makes the understanding of source geometry, coseismic rupture behaviors, and seismic cycle models difficult and presents challenges to seismic hazard assessment in developing cities and countries, particularly those located in intraplate regions.

The 2016 Gyeongju earthquake, which nucleated at a depth of about 14 km near the Yangsan fault (Kim *et al.*, 2016; Son *et al.*, 2018), resulted in strong ground shaking across the entire country and highlights the importance of earthquake response and seismic hazard research on the Korean Peninsula. Since early 2017, the Geological Research Center in the Korea Institute for Geosciences and Mineral Resources has carried out research projects associated with active fault mapping and/or paleoearthquakes along the major fault systems such as the Yangsan fault. For the Pohang earthquake, consequently, the research team responded flexibly to the shock and conducted detailed investigations of coseismic ground deformation with a multidisciplinary approach. A field survey team conducted surveys focused on mapping ground deformation utilizing postearthquake satellite- and unmanned aerial vehicle (UAV)-derived imagery. Initial InSAR data and real-time seismic records were used to complement field observations. Here, we describe near-field observations of coseismic ground deformation as well as bedrock faults in outcrop. We subsequently present a source model for the Pohang earthquake and discuss potential mechanisms of ground deformations.

Seismotectonic Setting of the Korean Peninsula

The southeastern part of the Korean Peninsula is located on the Eurasian plate and tectonically controlled by subduction of the adjacent Pacific and Philippine Sea plates (Fig. 1a), and collision of the Indian plate with Eurasia. Cenozoic tectonic deformation is primarily accommodated along two major structures, the Yangsan and Ulsan faults (Fig. 1b). Crustal deformation is also distributed across the eastern block of the Yangsan–Ulsan fault system (YUFS). Post-Oligocene southeastward directed rifting across this block resulted in northeast–southwest-trending extensional faults, and a number of structural basins were formed on the Cretaceous volcano-sedimentary succession (Yoon *et al.*, 2014; Son *et al.*, 2015). The Pohang area is also composed of middle Miocene sedimentary rocks with less than ~900 m of strata thickness on land (Song *et al.*, 2015). Since the Pliocene, the stress field has transitioned from extension to compression resulting in reactivation of pre-existing normal faults with reverse sense of motion (Kim and Park, 2006; Choi *et al.*, 2015).

Surface ruptures associated with Quaternary earthquakes, documented primarily by stratigraphic evidence, have been reported at about 60 sites along the YUFS as well as within the systems' eastern block (Kee *et al.*, 2009 and references therein; Fig. 1b). Paleoseismological studies indicate that earthquakes along the Yangsan fault are typically

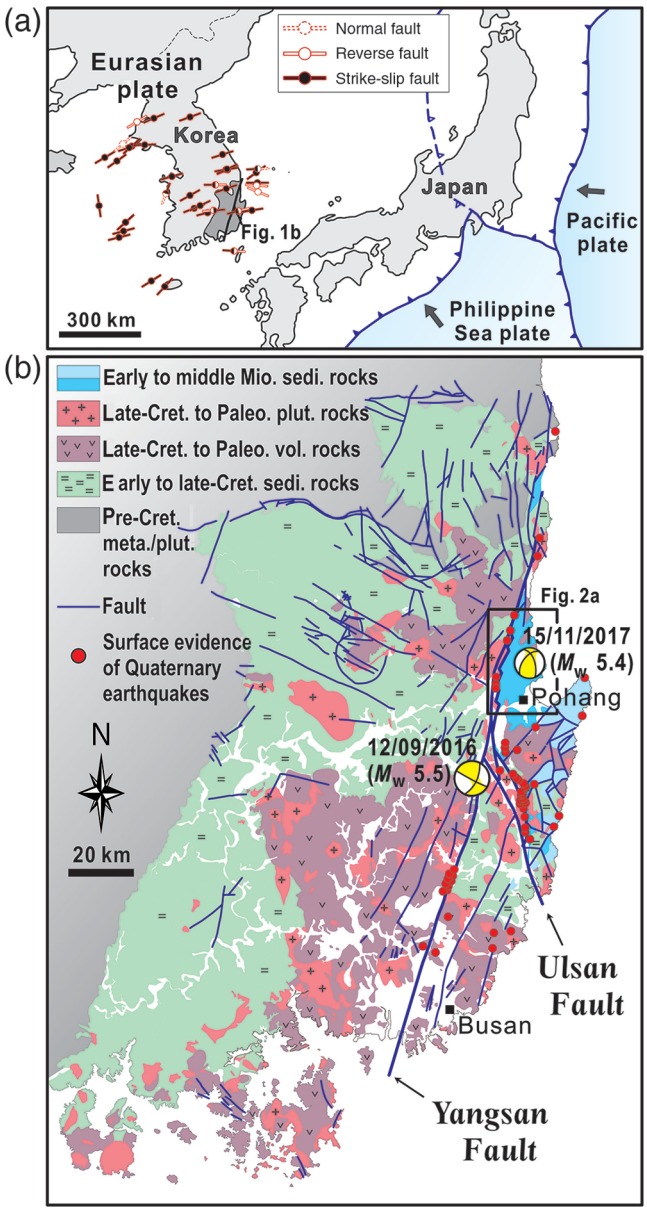

Figure 1. (a) Simplified tectonic map of study region. Bars indicate the maximum horizontal stress orientations with fault types determined by focal mechanisms from 40 earthquakes greater than or equal to M_w 3 from 1996 to 2014 (from the Saint Louis University Earthquake Center). (b) Geological map of the Gyeongsang basin, modified from the Korea Institute for Geosciences and Mineral Resources Geological Map. Circles indicate previously identified Quaternary surface faulting, primarily along the Yangsan–Ulsan fault system.

strike-slip (often with a component of dip slip), whereas reverse-slip earthquakes are more typical along the Ulsan fault and subsidiary faults to the east. The distribution of earthquake mechanisms is consistent with an east–west or east-northeast–west-southwest orientation of the maximum principal stress (Chang *et al.*, 2010; Soh *et al.*, 2018), and the direction has been persistent throughout the Quaternary (Jun and Jeon, 2010). This stress regime is also consistent with the principal compressive stress direction of 070°–090°

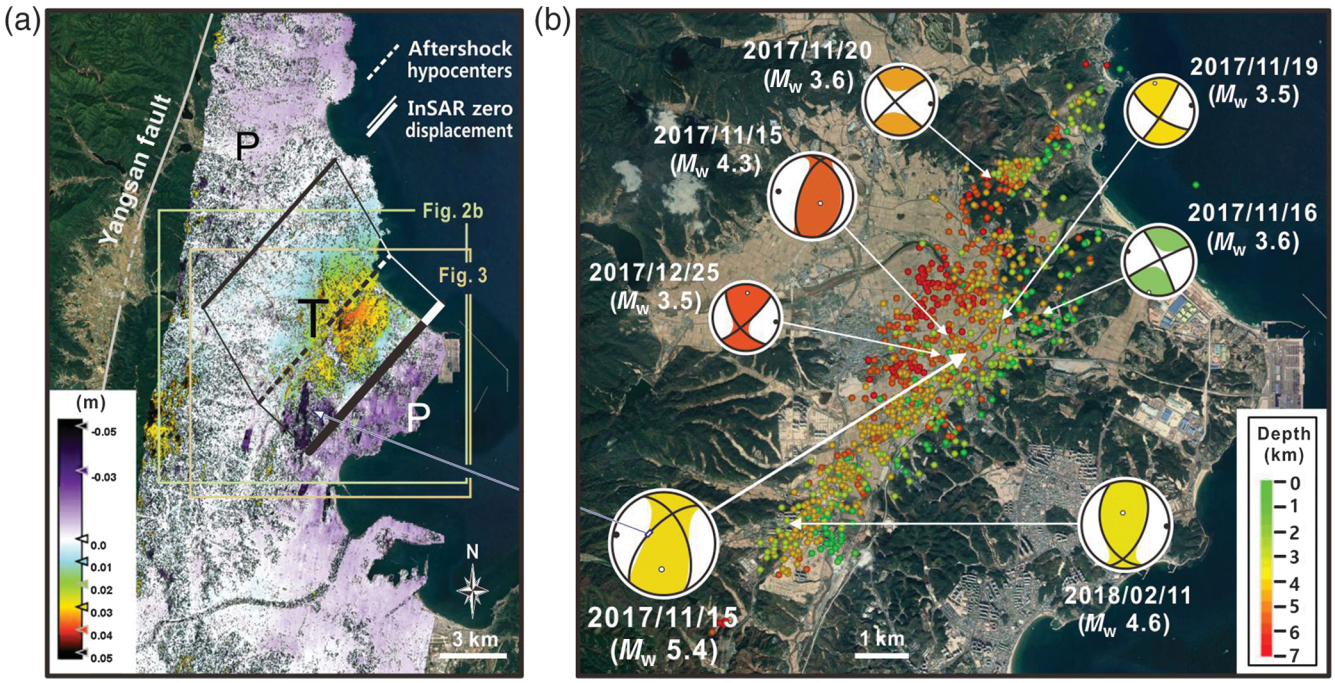

Figure 2. (a) Line-of-sight displacement map from Sentinel-1 Interferometric Synthetic Aperture Radar (InSAR) acquired on 4 and 16 November 2017. Positive values indicate uplift/easting of the ground while negative values are subsidence/westing. Distribution of ground displacements is consistent with a thrust focal mechanism for the mainshock. (b) Seismicity map of the 2017 Pohang earthquake sequence for the three months after the mainshock. Focal mechanisms are shown for the mainshock and major aftershocks greater than M_w 3.

estimated by focal mechanisms from 40 earthquakes greater than or equal to M_w 3 from 1996 to 2014 (data from Saint Louis University Earthquake Center; Fig. 1a).

Pohang Earthquake

Seismic Sequence

During the 100 days following the Pohang earthquake, more than 1300 seismic events were recorded on five temporary seismic stations (Fig. 2b), which were deployed around the epicenter and equipped with Q330HRS data loggers and Güralp CMG-40T sensors. About 1149 aftershocks were analyzed using cross correlation of *P* and *S* waveforms to determine the rupture plane. The results indicate that the main rupture occurred along a plane oriented N31°E–N50°E and dipping 60°–65° northwest (Cho, 2018). The direction of maximum horizontal stress by inversion of stress for the moment solutions is N80°W (Cho, 2018). That is slightly different from the known east-northeast–west-southwest maximum compression direction in the region. The seismically estimated fault plane correlates with the fault-plane solution determined from moment tensor inversion. Aftershock focal depths range from 2 to 7 km, and their along-fault distribution implies that the length of the main rupture was about 6 km. The two most significant ($M_w > 3$) aftershocks were triggered on neighboring fault segments: (1) the 20 November 2017 M_w 3.6 event on subvertical fault to the north and (2) the 11 February 2018 M_w 4.6 event on antithetically dipping fault to the southeast (Fig. 2b).

InSAR Analysis

The InSAR pair was acquired at 21:23 UTC on 4 and 16 November 2017 from Sentinel-1B satellite in descending polar orbit heading 190° and right looking so that the line of sight (LoS) from the antenna to the ground target is from east to west with an incidence angle of 40°. The data were processed by a SNAP program distributed freely from the European Space Agency. InSAR coherence was maintained in this heavily vegetated/cultivated area because (1) the rice paddy had already been harvested and the leaves of deciduous trees and bushes had already fallen in the late autumn, (2) the vegetation density of the mountains near the epicenter was sparse due to recent wild fires, and (3) the temporal and spatial baselines of the image pair were very short (12 days and 66.5 m, respectively).

Figure 2a is the displacement map associated with the Pohang earthquake in the LoS of the radar. About 4 cm uplift/easting displacement (red area) was estimated near the epicenter. A compressional quadrant (CQ shown as T in Fig. 2a) can be defined as a region with more than 2 cm displacement (green to red), which is roughly an oblique ellipse shape with a major axis of 6 km in the northeast–southwest direction, a minor axis of 4 km in the northwest–southeast direction, and an area of 16 km^2 (excluding ocean). Negative LoS displacement of up to −2 cm (purple) occurred in the southeastern part, which is thought to be a part of a dilatational quadrant (DQ shown as P in Fig. 2a). A white zone implying zero displacement lies between the CQ and

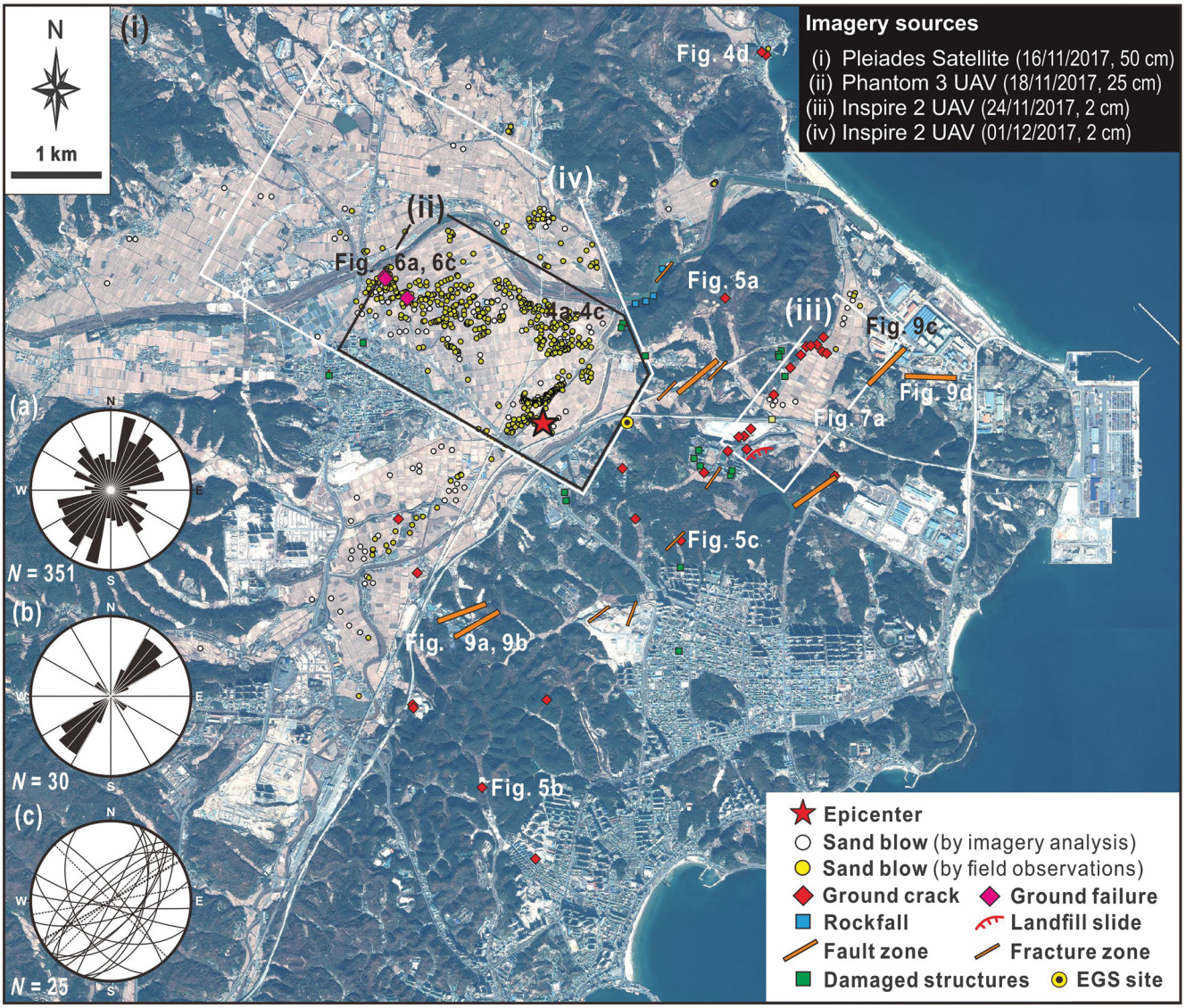

Figure 3. Map of surface deformations associated with the 2017 Pohang earthquake sequence. Deformational features and secondary effects of the earthquake include sand blows, ground cracks, rice paddy failures, rockfalls, and landfill slides. (Inset a) Orientations of sand blows (adapted from Gihm *et al.*, 2018) and (inset b) ground cracks are mostly parallel to (inset c) the direction of the main rupture as well as bedrock faults and fractures.

DQ with a direction of northeast–southwest. This zone corresponds with the surface projection of the earthquake rupture plane as determined by analysis of the seismic data. A slight DQ also appears in the northwest region of the CQ bordering with zero displacement (white), which completes a surface representation of a reverse fault. A linear slip inversion using the InSAR data suggests that an average coseismic slip of 15 cm occurred during the main rupture with the majority of slip concentrated northeast of the hypocenter rather than in the southwestern part (Song and Lee, 2018).

Coseismic Ground Deformation

In humid urban areas such as the Pohang region, it is important to quickly document coseismic ground deformation before features are removed by erosional processes and/or recovery and rebuilding efforts. To document ground deformation in the epicentral area of the Pohang earthquake, we utilized Pleiades high-resolution satellite (HRS) images, with a ground resolution of 0.5 m, which were acquired one day after the earthquake and offered by The International Charter (see Data and Resources). The dataset was complemented by UAV images, which have a ground resolution up to 0.02 m, particularly in rice fields. The imagery mapping includes the distribution of ground failures and/or sand blows that are larger than the ground resolution of the images (Fig. 3). The preliminary results were used for planning the field survey strategy, which was performed over a three-week period after the earthquake. During this survey, we observed and cataloged many sand

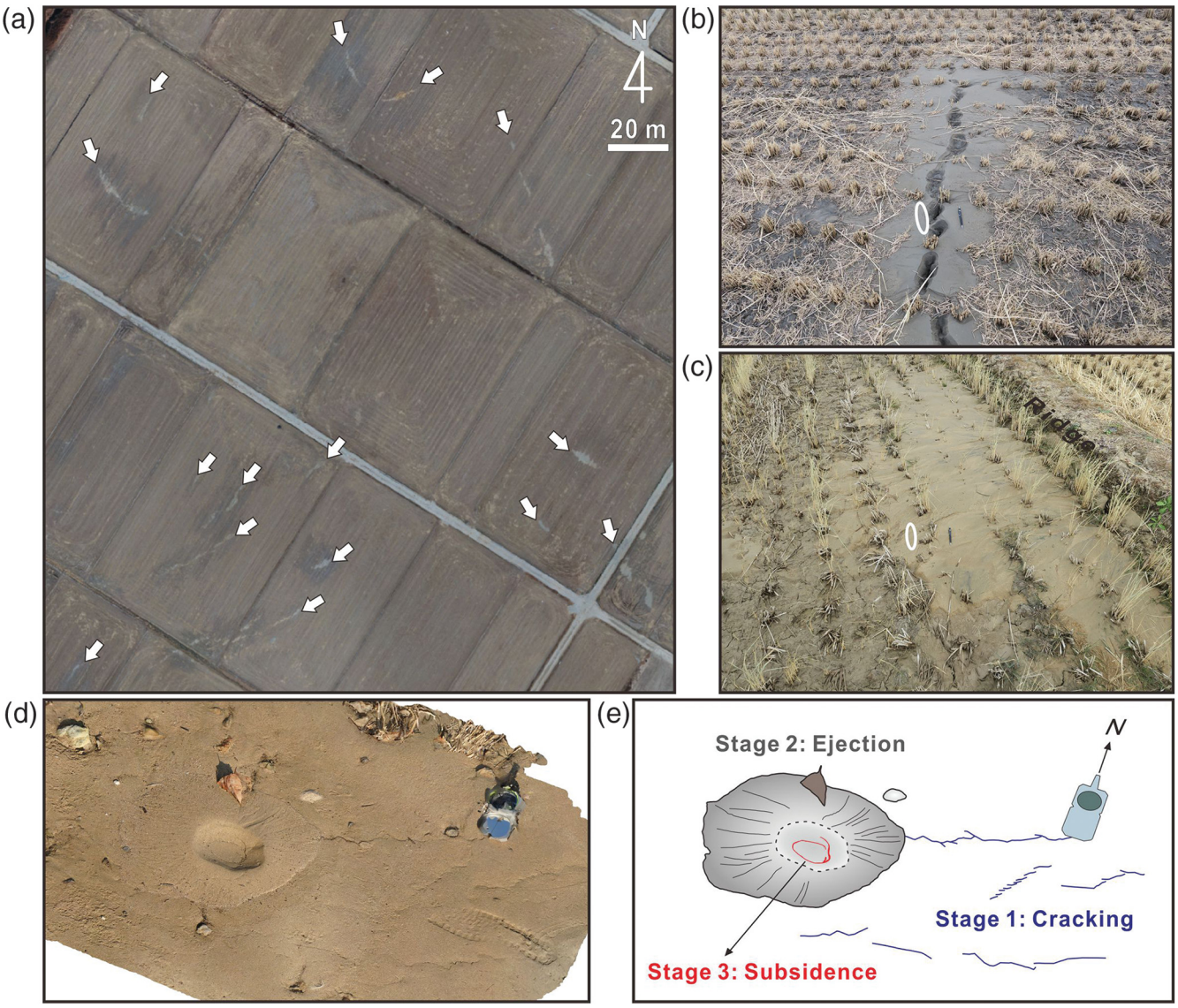

Figure 4. Examples of sand blows associated with the 2017 Pohang earthquake. (a) A conjugate system of sand blows on rice fields identified by unmanned aerial vehicle (UAV)-derived images (ground resolution of ~2 cm). (b,c) Field photos showing sand blows erupted through ground cracks or man-made structures (e.g., ridges; adapted from Gihm *et al.*, 2018). Circles indicate pencil for scale. (d,e) A 3D image and sketch of a sand volcano ejected through a ground crack on the beach.

blows, ground cracks, deformed rice paddies, landfill slides, and rockfalls (Fig. 3). Here, we provide an overview of our observations for each type of ground deformation.

Sand Blows. Sand blows (or sand volcanoes) are associated with soil liquefaction and the ejection of fluidized sand onto the surface during and immediately after an earthquake. On the HRS images, we observed locations that were flooded by water ejected from the subsurface, especially on rice fields around the epicenter (Fig. 3). The preliminary observations were used to designate areas for field investigation that verified the presence of sand blows. In total, the sand blow dataset includes 351 sites (Gihm *et al.*, 2018). It is noteworthy that, although a few of the targeted sites did not contain evidence of sand blows, the results of our imagery mapping are well correlated with the distribution of the sand blows mapped in the field.

The sand blows exhibit linear patterns on the surface (Fig. 4a–c), and average 5.44 m in length, with several sand blows up to 70 m long (Gihm *et al.*, 2018). Overall, the linear patterns of sand blows are subparallel or subperpendicular to the earthquake rupture (Fig. 3, inset a). This may imply that coseismic ground cracks, often linear features, provide a pathway for ejecting sand. This process seems to be common for other types of sand blows. For example, Figure 4d shows a conical-shaped sand volcano on a beach that formed in response to a sequence of processes (Fig. 4e) including: (1) cracking with a preferred orientation of northeast, (2) ejection of sand at the lateral tip of the crack (see a fallen leaf arrested by sands), and (3) subsidence of the central part.

The majority of the sand blows are concentrated on the northwestern side of the rupture and within a 3 km radius of the epicenter (Fig. 3). This asymmetric distribution may be due to the existence of unconsolidated sediments on the northwestern side of the epicenter, which are susceptible to liquefaction and ground-motion amplification. We infer that the distribution of sand blows is a function of the location of coseismic ground cracks in areas of liquefiable sediments.

Ground Cracks. In addition to sand blows, the Pohang earthquake produced widespread ground cracking around the epicenter (within a radius of ~3 km). The majority of ground crack features are concentrated on the eastern side of the epicenter, particularly along the margin between mountainous areas and rice fields (Fig. 3). At several locations northwest of the epicenter, we observed linear mound-like features on rice paddies. Crack clusters occurred mainly on landfill sites.

In the mountainous areas east of the epicenter, conjugate extensional fractures were observed in Tertiary sedimentary rocks (Fig. 5a). At some sites, surficial cracking caused small-scale rockfalls on road-cut sections during the earthquake (Fig. 5b). En echelon arrays of ground cracks were observed on unconsolidated ground (Fig. 5c–e). The orientations of en echelon cracking zones are typically northeast–southwest (Fig. 3, inset b), subparallel to the earthquake rupture. Some of the en echelon cracks show a left-stepping geometry consistent with a component of right-lateral shear, which is the same with the sense of strike-slip component associated with the Pohang earthquake (Fig. 5c). Some of them, however, exhibit a right-stepping geometry indicating an opposite strike-slip sense to the main rupture (Fig. 5e,f).

At a few sites northwest of the epicenter, ground deformation was observed on rice fields. One example is a linear mound-like feature caused by cracking and lifting up of a dry topsoil layer of the rice paddy (Fig. 6a). Although individual cracks of the deformation feature trend subparallel or orthogonal to furrows on the rice paddy, the overall orientation of the feature is subparallel to the Pohang earthquake rupture. A digital elevation model (DEM), generated with the Agisoft Photoscan program, indicates about 0.5 m of vertical deformation (Fig. 6b). These features are similar in appearance and morphology to mole tracks caused by surface ruptures but are not long or continuous. Another example shows about 10 cm of vertical deformation along a single vertical crack, and the amount of deformation is similar to the thickness of a dry topsoil layer (Fig. 6c). The orientation is subparallel to both furrows on the rice paddy and the Pohang earthquake rupture. In the field, we confirm that small empty cavities formed just below the deformed topsoil layer. Based on the InSAR analysis, there was almost no surface displacement around the sites of these vertical soil deformations (Figs. 2a and 3). We infer that the local pop-up-like deformation of the soil is the result of horizontal ground shaking of rigid soil blocks, and not primary tectonic deformation (i.e., not surface rupture). This is supported by locations and orientations of the deformational features, which are similar to the sand blows caused by ground shaking. Sun cracks with a major direction parallel to furrow are common on rice fields after harvest season, after November in the Pohang area. Hence, the preferred orientation of individual cracks may be also partially controlled by such pre-existing nonseismic cracks.

A series of ground cracks were observed within an about 400-m-wide zone centered around Handong University, one of the areas most damaged by the Pohang earthquake (Fig. 7a). A number of buildings on the University campus and in neighboring villages suffered from significant damage (Fig. 7b,e); a bridge was partially closed due to damaged piers (Fig. 7a). Within this zone, ground cracks were recognized on rice fields, unpaved and cemented roads, and construction sites (Figs. 5d–f and 7d,e). Most of these cracks show a preferred northeast–southwest orientation.

Numerous cracks were widely distributed on landfill sites, which are located within the highly damaged zone (Fig. 7). Some cracks are characterized by dimensions of tens of meters in length and a few centimeters in vertical separation. Figure 8 shows an example of ground deformation on and around a landfill site. Digital orthophotos and DEM data were produced by UAV-derived images, and informed detailed mapping of the ground cracks. At the southeastern side of the landfill, a rice paddy exhibited an uneven and folded relief, characterized by curvy and anastomosing crack patterns (Fig. 8b). Extensional cracks were observed north of the deformed ground. Many cracks were formed on the landfill cap, which is about 20 m higher than an undeformed rice paddy (a datum surface in Fig. 8b) (Fig. 8c,d). The cracks show a fan-shaped distribution in map view (Fig. 8c), even though they are predominantly oriented to the northeast–southwest. Vertical separation along the cracks indicates that the southeastern side moved down relative to the northwestern side (Fig. 8d). The vertical deformation is shown in Figure 8e. In particular, topographical profiles indicate that the northwestern side of the rice paddy, which was originally a horizontal surface, was warped upward more than 1 m (Fig. 8e). The lateral extent of the folded and tilted ground was confined to the rice paddy adjacent to the landfill. Thus, the ground deformation on the rice paddy appears to be a local effect of landsliding generated by strong ground shaking. We infer that the observed ground deformation both on the landfill cap (extension) and on the rice paddy (compression) resulted from a local landfill sliding, and not primary tectonic deformation during the earthquake.

Discussion

Source Geometry

After an earthquake, it is important to observe and record surface ruptures and ground deformation to help assess the impact of the mainshock and better understand ongoing seismic sequences and their related earthquake hazards (Parameswaran *et al.*, 2015). In the case of the Pohang

Figure 5. Photographs of ground cracks induced by the 2017 Pohang earthquake (locations of each photograph shown in Fig. 3): (a,b) block jointing in bedrocks and (b) its related rockfalls. En echelon cracks on the dirt of (c) on a playground, (d,e) along a road, and (f) across a paved road. Trends of the each en echelon cracking zone are subparallel to the orientation of the main rupture. Circles indicate compass for scale.

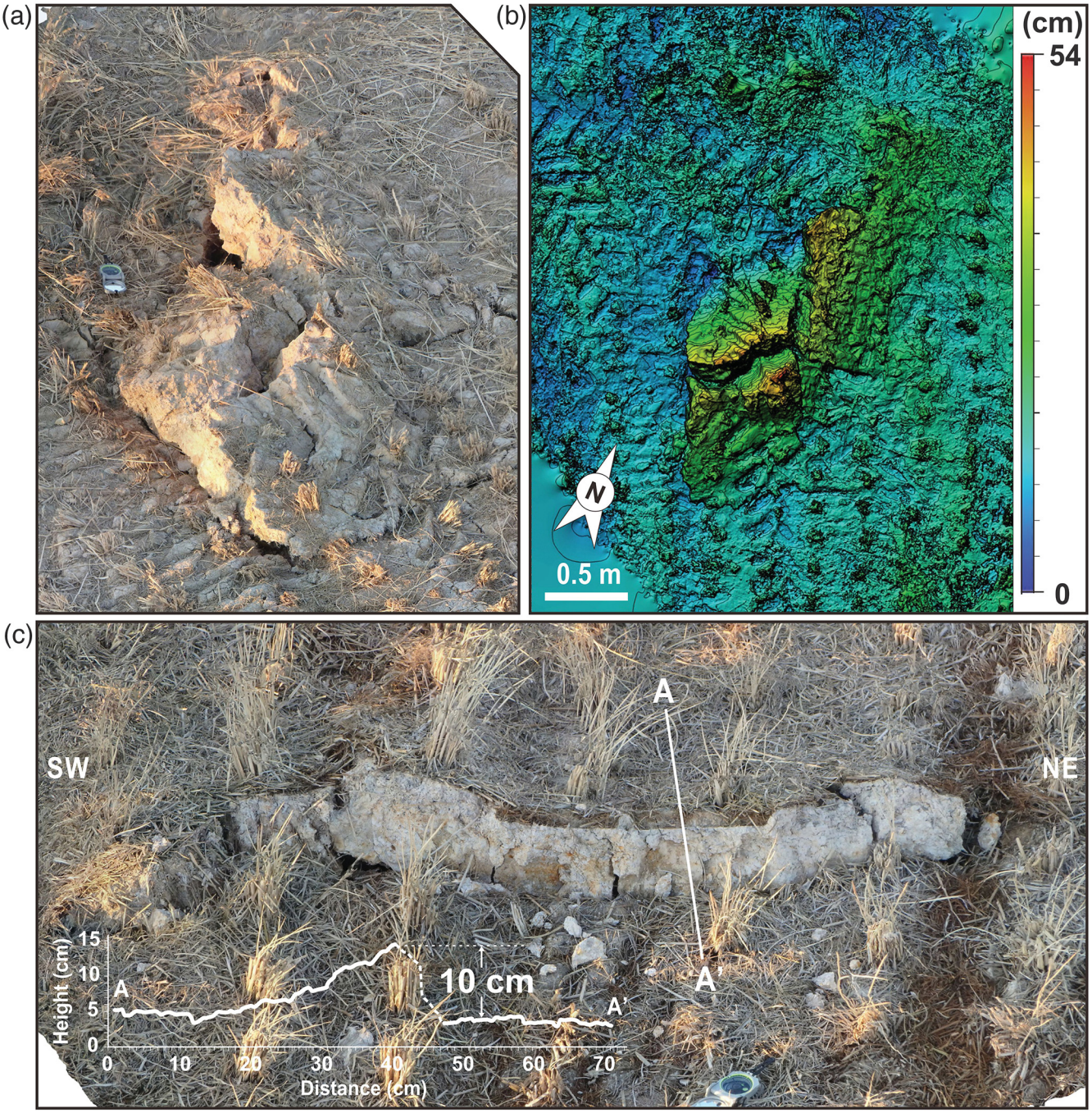

Figure 6. 3D images of rice paddies deformed by the 2017 Pohang earthquake. (a) A structural pattern similar to mole tracks indicating a potential lateral component of motion during uplift. (b) A digital elevation model produced by Photoscan displaying about a half-meter of uplift across a pop-up structure. (c) A vertical profile across a mole track showing about 10 cm of vertical deformation.

earthquake, however, the absence of coseismic surface rupture made characterization of the source geometry difficult. Moreover, there were no mapped active faults near the epicenter. Postearthquake field surveys provide the opportunity to directly observe coseismic ground deformation and pre-existing fault structures in outcrop. These observations can be compared to other near- and far-field observations to develop a better understanding of the source geometry. In the field, we observed faults and/or fracture zones at sites around the epicenter (Figs. 3 and 9). Here, we take advantage of geometric features of the pre-existing fault structures as well as the map of coseismic ground deformation to examine the source geometry of the Pohang earthquake.

Pre-existing faults are exposed in Miocene mudstone bedrock in the foothills east of the epicenter (Fig. 3). Northeast–southwest-trending high-angle normal faults are dominant around the epicenter (Figs. 3, inset c, and 9a–c). The sense of fault slip is supported by stratigraphic offsets

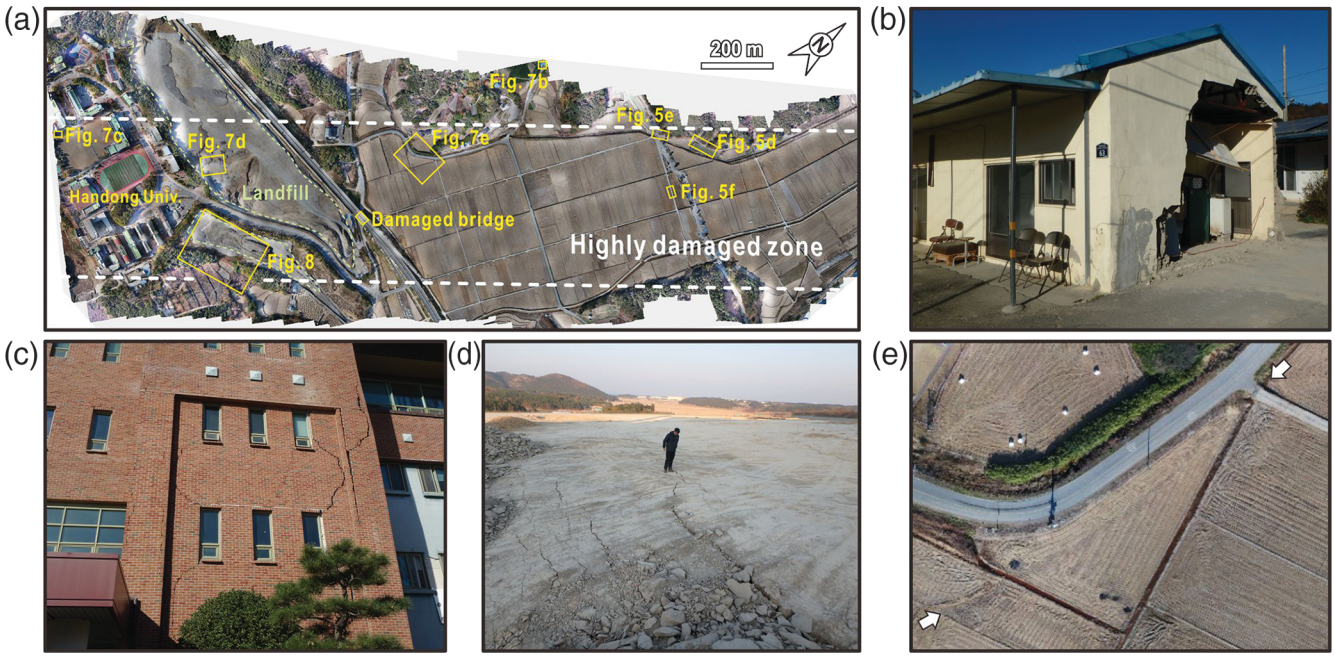

Figure 7. (a) A location map imaged by UAV-derived photos showing (b,c) field examples of structural damage and (d,e) surficial cracking associated with the 2017 Pohang earthquake. These features are along the projection of the blind earthquake rupture (see details in the Discussion section).

and subvertical extensional fractures in outcrop. At each outcrop, the main fault commonly dips to the southeast except in a few cases. The majority of the faults are associated with secondary faults having parallel strikes but opposite dips, that is, antithetic faults (Fig. 9a,b). Around one of these faults, we observed redeposited mudstone as well as highly tilted and/or folded unconsolidated beach sediments implying Quaternary reactivation of the fault (Fig. 9c). The young sediments were also cut by a nearly east–west-trending normal fault, which is consistent with the present-day tectonic stress field (Fig. 9d).

The basin-fill deposits of the Pohang basin accumulated during the Miocene in extensional basins related to normal faulting along southeast-dipping faults (Son *et al.*, 2015). Based on seismic records and an InSAR-constrained displacement model, we infer that the main rupture during the Pohang earthquake occurred along a northwest-dipping fault (Fig. 2). Coseismic ground cracks are generally concentrated along the surface projection of the main rupture and predominantly on the hanging-wall block (Fig. 10). Thus, we infer that the earthquake rupture occurred by reactivation of an antithetic fault belonging the northeast–southwest-trending, southeast-dipping high-angle fault system.

Two aftershocks occurred at both lateral tips of the main rupture (Fig. 2b). To the north, an aftershock occurred on a subvertical fault showing a left-stepping geometry subparallel to the main rupture. The distance between the two faults is about 2 km. To the southwest, an aftershock ruptured a fault with an opposite dip to the main rupture. The fault system associated with the Pohang earthquake sequence, therefore, appears to be composed of discontinuous fault segments separated by stepping (or relay) geometry. This is in contrast to other more continuous major strike-slip fault systems in the surrounding areas, that is, the YUFS. We infer that the fault steps may have acted to terminate the propagating coseismic main rupture of the Pohang earthquake. Fault steps represent structural discontinuities that can provide barriers to rupture propagation (Wesnousky, 2006). Additionally, the minimum depth of aftershocks recorded by temporary seismic network is less than 1 km, similar to the thickness of the Miocene mudstone. This suggests that stratigraphic discontinuities and/or vertical variations in structural geometries may contribute toward limiting the up-dip propagation of the rupture (Fig. 10).

Causes of Ground Failures

The secondary ground deformation generated by the Pohang earthquake was a direct result of ground shaking and site effects, and represents a second-order seismic hazard from moderate-sized earthquakes in the Pohang basin. Our mapping of coseismic ground cracks generated during the Pohang earthquake indicates that the cracks exhibit spatially distinguishable distribution including (1) most of the cracks are concentrated on the northwestern side of the epicenter, and (2) some cracks are clustered along the inferred up-dip projection of the blind rupture. Orientations of the ground cracks are primarily parallel, and in some cases perpendicular to the main rupture (Fig. 3, insets a,b). Here, we examine the relations between the spatially

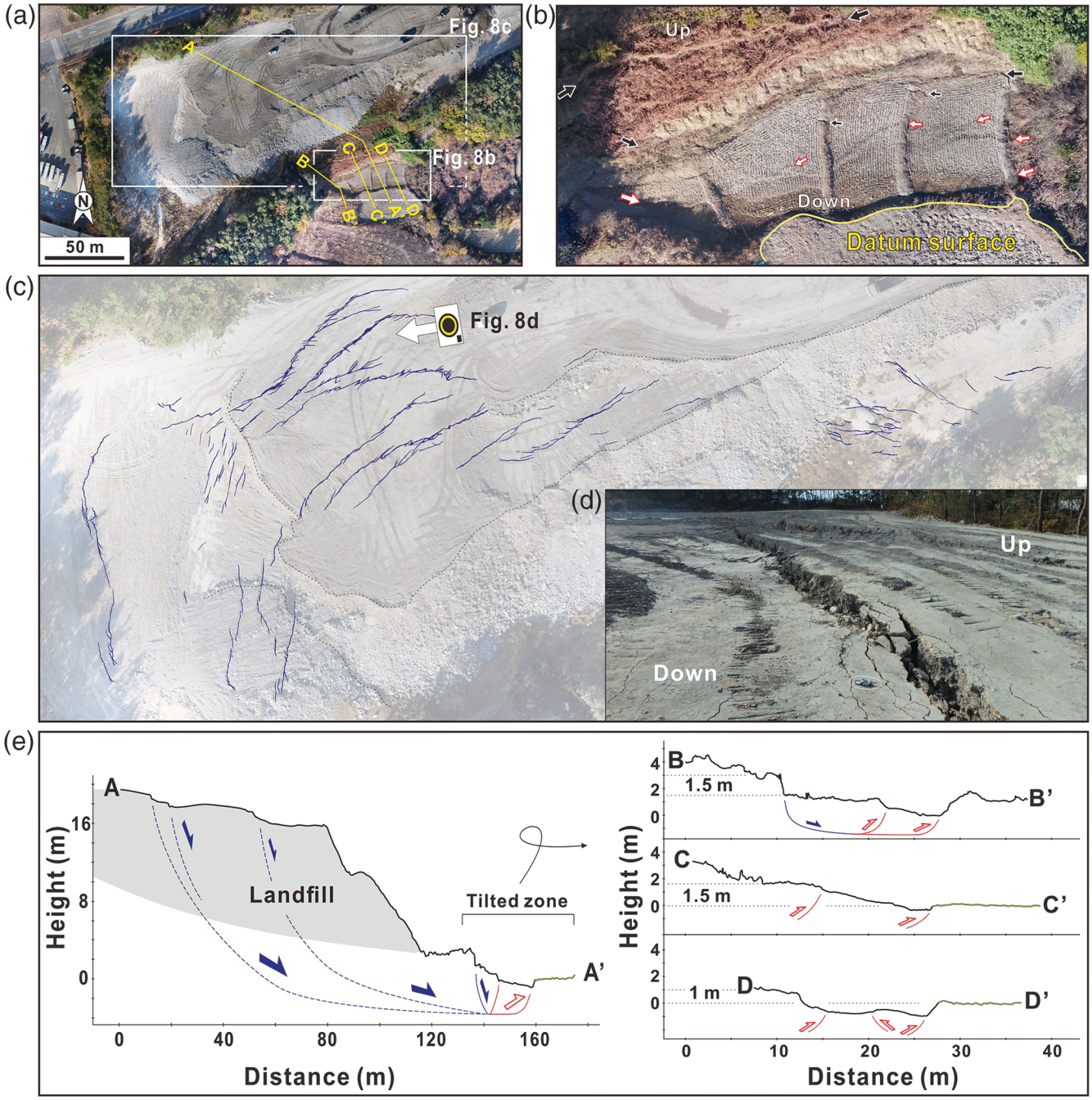

Figure 8. (a) An example of landfill failure induced by the 2017 Pohang earthquake, imaged by UAV-derived photography. (b) Compressional features (unfilled white arrows) such as folded ground on a tilted rice paddy and extensional cracks (filled black arrows) in the northwestern side. These features formed on the ground next to, not on the surface of, a landfill. (c) Arc-shaped cracks on the landfill surface indicating downslope movement of unconsolidated landfill material and possibly mass wasting associated with ground shaking. (d) A photography showing cracks and their related vertical deformation in a detail view. (e) Vertical profiles (A–D) across the landfill slide.

distinguishable distribution of ground failures and coseismic rupture processes.

On rice fields northwest of the epicenter, numerous sand blows exhibit a linear pattern suggesting that vertical ground cracks were a major pathway for ejecting sand onto the surface. The cracks are highly concentrated within a 3 km radius of the epicenter, and ground cracking was often associated with local pop-up deformation. The InSAR data suggest that, in these areas, there was almost no vertical deformation of the ground (Fig. 2a). Figure 11a shows the horizontal component of the peak ground acceleration produced by the Pohang earthquake, and indicates that lateral strong motion near the epicenter was more than 400 cm/s^2. We attribute the ground cracks on the rice fields to seismic shaking of unconsolidated sediments, particularly horizontal ground motions produced by *S* waves and surface waves (Fig. 10).

Figure 9. Photographs and simple sketches for fault outcrops in the vicinity of the epicenter of the 2017 Pohang earthquake. (a,b) Field photos showing a conjugate geometry of northeast-trending normal faults. Circles indicate geologic hammer for scale. (c,d) Road-cut sections, imaged by UAV-derived photos, showing unconsolidated sediments cut by faults that indicate the occurrence of previous paleoearthquakes.

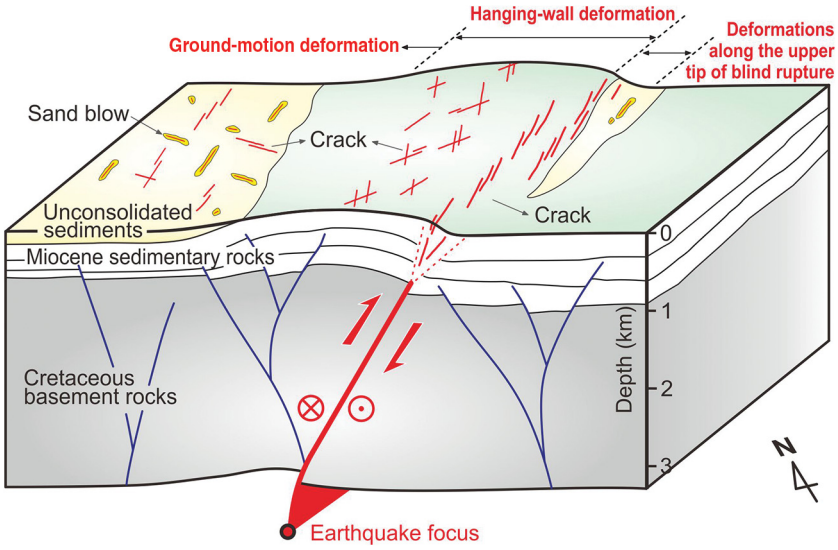

Figure 10. A schematic diagram showing the distribution of surface deformation across the 2017 Pohang earthquake rupture and proposed mechanism associated with blind oblique-slip including reverse-slip component and their related surface folding.

In the foothills east of the epicenter, conjugate pairs of vertical cracks were the typical geometry of ground failures. This area corresponds with the uplifted hanging-wall block of the main rupture. The maximum vertical displacement ranges from 4 to 6 cm according to the InSAR analysis (Fig. 2a) and the surface displacement field constrained by a linear slip inversion of the InSAR data (Fig. 11b; Song and Lee, 2018). Thus, the cracks within the uplifted hills appear to be related to brittle extension along the crest of the folded surface (Fig. 10).

Additional ground cracks are clustered within a northeast–southwest-trending zone several hundred meters wide and are associated with a landslide in a landfill (Fig. 8). The location of this highly deformed zone corresponds with a boundary between areas showing two different patterns of both horizontal and vertical surface displacements along the surface projection of the blind rupture (Fig. 11b). This suggests that distributed deformation related to the propagating rupture tip at shallow depth may influence the distribution of ground cracking (Fig. 10). Thus, the mapping results demonstrate that earthquake-induced ground failures may be influenced by both ground shaking (dynamic strain) and processes of blind faulting (static strain), involving reverse slip and related surface folding (Philip and Meghraoui, 1983).

Implications for Earthquake Hazards

Evaluating earthquake hazards in intraplate regions such as Korea is hindered by relatively low rates of tectonic deformation and broad uncertainties in estimating the size of potential earthquakes. This is in contrast to tectonically active regions where seismic hazard assessments benefit from better characterized faults and relatively less uncertainty in fault rupture parameters. The Pohang earthquake sequence was generated by reactivation of a pre-existing fault system that was not previously mapped or recognized as neotectonically active. Thus, our documentation of secondary deformation caused by the Pohang earthquake provides information that contributes toward a better understanding of potential future earthquake damage. The

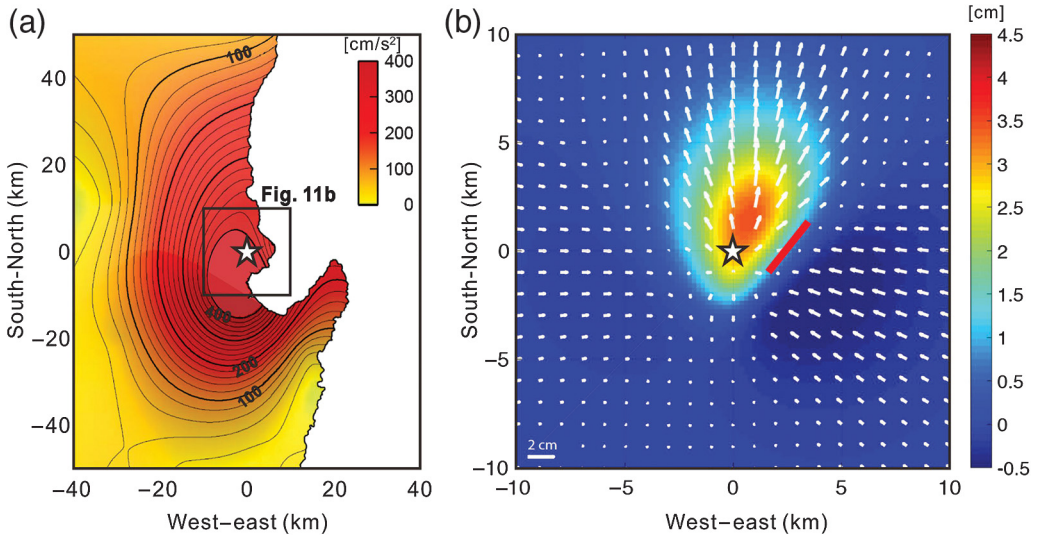

Figure 11. Distribution maps of (a) horizontal component of the peak ground acceleration and (b) both horizontal (arrows) and vertical components (color contour) of predicted ground displacement (adapted from Song and Lee, 2018) associated with the 2017 Pohong earthquake. Stars indicate the epicenter. A red line in (b) indicates the projection of the blind rupture, and this area corresponds with the location of the highly damaged zone shown in Figure 7a.

information also contributes toward the establishment of seismic rick policies in the Pohang area and any other regions situated in similar environments.

The Pohang earthquake demonstrated that coseismic ruptures, directly accommodating the released seismic energy, could not propagate onto the surface even though it was a moderate-sized earthquake that occurs at a very shallow depth. Instead, the second-order ground deformation related to ground shaking was the primary effect and responsible for the majority of the damage. The distributed ground failures are mainly controlled by geometry-dependent rupture processes on pre-existing faults, both by static and dynamic strain generated by an earthquake (Manga *et al.*, 2016), as well as local ground conditions. Landfills and other areas with anthropogenically modified soils were affected by landsliding and/or other ground deformation that may have been related to amplification of ground motions in those areas. These observations and interpretations are useful for earthquake mitigation planning, particularly for urban areas in Korea.

In this article, we limit our focus to the coseismic ground deformation. In the field surveys, however, we also observed potential tectonic surface deformation during the Quaternary such as faulted or folded unconsolidated beach sediments (Fig. 9c,d). Around the Pohang area, paleoseismological studies have previously reported liquefaction associated with paleoearthquakes (Korea Meteorological Administration, 2012; Lee *et al.*, 2014). These records of earthquake-generated deformation suggest the Pohang area is tectonically active. Tectonically active structures have the potential to produce damaging earthquakes. Thus, in addition to documenting secondary effects, future advances in seismic hazard assessment in Korea are dependent on detailed paleoseismic and geomorphic studies of active faults and deformed landforms.

Conclusions

We obtained the details of coseismic ground deformation associated with the 2017 Pohang earthquake sequence based on the high-resolution near-field observations. The results show that rupture-parallel ground cracks exist over the entire area surrounding the epicenter, but their mechanisms vary depending on locations in reference to the rupture processes. Soft ground conditions play a key role in influencing the type and distribution of ground deformation. This study provides insights into the source mechanism of the 2017 Pohang earthquake related with reverse reactivations of pre-existing normal faults in the modern stress field. The faults in the vicinity of Pohang area were previously not considered active and only recognized as a system of segmented normal faults. This study shows that the fault system has the potential for future earthquakes, possibly larger events, and emphasizes the necessity of paleoseismological approaches for better assessment of potential damaging earthquakes. Finally, the results highlight the importance of documenting ground deformation to better understand secondary effects of earthquakes and source geometry, as well as to improve seismic hazards assessments.

Data and Resources

The maximum horizontal stress orientations database was searched using http://www.eas.slu.edu/eqc/eqc_mt/MECH.KR/ (last accessed June 2018). Geological map of the Gyeongsang basin was modified from http://mgeo.kigam.re.kr/ (last accessed June 2018). High-resolution satellite image was offered by The International Charter (https://disasterscharter.org/, last accessed June 2018).

Acknowledgments

This research was supported by Basic Science Research Program through the National Research Foundation of Korea (NRF) funded by the Ministry of Education, Science and Technology (2018M3D7A-1052897). Satellite images were offered by The International Charter, Korea Aerospace Research Institute, National Disaster Management Research Institute, and European Space Agency. The authors thank G. H. Ji, Y.-S. Kim, S.-I. Park, I.-G. Hwang, W.-S. Kee, M. Son, and H. I. Cho for their contribution to this work. The authors thank M. Shirzaei, R. D. Koehler, and Associate Editor R. Grapenthin for their constructive reviews that greatly improved the article.

References

Ainscoe, E. A., J. R. Elliott, A. Copley, T. J. Craig, T. Li, B. E. Parsons, and R. T. Walker (2017). Blind thrusting, surface folding, and the development of geological structure in the M_W 6.3 2015 Pishan (China) earthquake, *J. Geophys. Res.* **122,** doi: 10.1002/2017JB014268.

Champenois, J., S. Baize, M. Vallee, H. Jomard, A. Alvarado, P. Espin, G. Ekstom, and L. Audin (2017). Evidences of surface rupture associated with a low-magnitude (M_W 5.0) shallow earthquake in the Ecuadorian Andes, *J. Geophys. Res.* **122,** 8446–8458, doi: 10.1002/2017JB013928.

Chang, C., J. B. Lee, and T.-S. Kang (2010). Interaction between regional stress state and faults: Complementary analysis of borehole in situ stress and earthquake focal mechanism in southeastern Korea, *Tectonophysics* **485,** 164–177.

Cho, C. S. (2018). Characteristics of Pohang earthquake (M_w 5.4) occurred near developing geothermal well and relative relocations of aftershocks using hierarchical clustering, *Geophys. Res. Abstr.* **20,** EGU2018–6850.

Choi, J.-H., S.-J. Yang, S.-R. Han, and Y.-S. Kim (2015). Fault zone evolution during Cenozoic tectonic inversion in SE Korea, *J. Asian Earth Sci.* **98,** 167–177.

Gihm, Y. S., S. W. Kim, K. Ko, J.-H. Choi, H. Bae, P. S. Hong, Y. Lee, H. Lee, K. Jin, S.-J. Choi, *et al.* (2018). Paleoseismological implications of liquefaction-induced structures caused by the 2017 Pohang earthquake, *Geosci. J.* **22,** no. 6, 871–880, doi: 10.1007/s12303-018-0051-y.

Grandin, R., M. Vallee, and R. Lacassin (2017). Rupture process of the M_W 5.8 Pawnee, Oklahoma, earthquake from Sentinel-1 InSAR and seismological data, *Seismol. Res. Lett.* **88,** no. 4, doi: 10.1785/0220160226.

Grigoli, F., S. Cesca, A. P. Rinaldi, A. Manconi, J. A. López-Comino, J. F. Clinton, R. Westaway, C. Cauzzi, T. Dahm, and S. Wiemer (2018). The November 2017 M_W 5.5 Pohang earthquake: A possible case of induced seismicity in South Korea, *Science* **360,** 1003–1006, doi: 10.1126/science.aat2010.

Jun, M.-S., and J. S. Jeon (2010). Focal mechanism in and around the Korean Peninsula, *Jigu-Mulli-wa-Mulli-Tamsa* **13,** 198–202 (in Korean with English abstract).

Kee, W.-S., Y. H. Kihm, H. Lee, D. L. Cho, B. C. Kim, K.-Y. Song, H. J. Koh, S. R. Lee, Y.-K. Yeon, S. Hwang, *et al.* (2009). Evaluation and database construction of Quaternary faults in SE Korea, Korea Institute for Geosciences and Mineral Resources, IP2006-047-2009(1) (in Korean).

Kim, K.-H., T.-S. Kang, J. Rhie, Y. Kim, Y. Park, and S. Y. Kang (2016). The 12 September 2016 Gyeongju earthquakes: 2. Temporary seismic network for monitoring aftershocks, *Geosci. J.* **20,** no. 6, 753–757, doi: 10.1007/s12303-016-0034-9.

Kim, K.-H., J.-H. Ree, Y. H. Kim, S. Kim, and S. Y. Kang (2018). Assessing whether the 2017 M_W 5.4 Pohang earthquake in South Korea was an induced event, *Science* **360,** 26, doi: 10.1126/science.aat6081.

Kim, Y.-S., and J. Park (2006). Cenozoic deformation history of the area around Yangnam-Yangbuk, SE Korea and its tectonic significance, *J. Asian Earth Sci.* **26,** 503–517.

Korea Meteorological Administration (2012). *Historical Earthquake Records in Korea (2~1904)*, Korea Meteorological Administration Press, Seoul, Korea (in Korean).

Kyung, J. B. (2003). Paleoseismology of the Yangsan fault, southeastern part of Korean peninsula, *Ann. Geophys.* **46,** 149–165.

Lee, H. I., I. S. Paik, H.-C. Kang, and J. H. Chun (2014). Occurrences and origins of soft-sediment deformation structures in the late Pleistocene marine terrace deposits of the southeastern coast of Korea, *Geosci. J.* **18,** 149–165.

Lee, K., and S. H. Na (1983). A study of microearthquake activity of the Yangsan fault, *J. Geol. Soc. Korea* **19,** no. 3, 127–135 (in Korean with English abstract).

Lekkas, E., S. Mavroulis, P. Carydis, and V. Alexoudi (2018). The 17 November 2015 M_W 6.4 Lefkas (Ionian Sea, western Greece) earthquake: Impact on environment and buildings, *Geotech. Geol. Eng.* **36,** no. 4, 2109–2142, doi: 10.1007/s10706-018-0452-8.

Manga, M., C.-Y. Wang, and M. Shirzaei (2016). Increased stream discharge after the 3 September 2016 M_W 5.8 Pawnee, Oklahoma earthquake, *Geophys. Res. Lett.* **43,** 11,588–11,594, doi: 10.1002/2016GL071268.

Parameswaran, R. M., T. Natarajan, K. Rajendran, C. P. Rajendran, R. Mallick, M. Wood, and H. C. Lekhak (2015). Seismotectonics of the April–May 2015 Nepal earthquakes: An assessment based on the aftershock patterns, surface effects and deformational characteristics, *J. Asian Earth Sci.* **111,** 161–174.

Philip, H., and M. Meghraoui (1983). Structural analysis and interpretation of the surface deformations of the El Asnam earthquake of October 10, 1980, *Tectonics* **2,** no. 1, 17–49.

Soh, I., C. Chang, J. Lee, T.-K. Hong, and E.-S. Park (2018). Tectonic stress orientations and magnitudes, and friction of faults, deduced from earthquake focal mechanism inversions over the Korean Peninsula, *Geophys. J. Int.* **213,** 1360–1373.

Son, M., C. S. Cho, J. S. Shin, H.-M. Rhee, and D.-H. Sheen (2018). Spatiotemporal distribution of events during the first three months of the 2016 Gyeongju, Korea, earthquake sequence, *Bull. Seismol. Soc. Am.* **108,** no. 1, 210–217, doi: 10.1785/0120170107.

Son, M., C. W. Song, M.-C. Kim, Y. Cheon, H. Cho, and Y. K. Sohn (2015). Miocene tectonic evolution of the basins and fault systems, SE Korea: Dextral, simple shear during the East Sea (Sea of Japan) opening, *J. Geol. Soc.* **172,** 664–680, doi: 10.1144/jgs2014-079.

Song, C. W., M. Son, Y. K. Sohn, R. Han, Y. J. Shinn, and J.-C. Kim (2015). A study on potential geologic facility sites for carbon dioxide storage in the Miocene Pohang basin, SE Korea, *J. Geol. Soc. Korea* **51,** no. 1, 53–66 (in Korean with English abstract).

Song, S. G., and H. Lee (2018). Static slip model of the 2017 M_w 5.4 Pohang, South Korea, earthquake, constrained by InSAR data, *Seismol. Res. Lett.* **90,** no. 1, 140–148, doi: 10.1785/0220180156.

Talebian, M., E. J. Fielding, G. J. Funning, M. Ghorashi, J. Jackson, H. Nazari, B. Parsons, K. Priestley, P. A. Rosen, R. Walker, *et al.* (2004). The 2003 Bam (Iran) earthquake: Rupture of a blind strike-slip fault, *Geophys. Res. Lett.* **31,** L11611, doi: 10.1029/2004GL020058.

Wesnousky, S. (2006). Predicting the endpoints of earthquake ruptures, *Nature* **444,** no. 7117, 358–360.

Yoon, S. H., Y. K. Sohn, and S. K. Chough (2014). Tectonic, sedimentary, and volcanic evolution of a back-arc basin in the East Sea (Sea of Japan), *Mar. Geol.* **352,** 70–88.

Geology Division
Korea Institute for Geosciences and Mineral Resources
Daejeon 34132, Republic of Korea
cjh9521@kigam.re.kr
kkt@kigam.re.kr
naress@kigam.re.kr
nemex@kigam.re.kr
sgsong@kigam.re.kr
bhk1990@kigam.re.kr
sungwon@kigam.re.kr
sjchoi@kigam.re.kr
leesr@kigam.re.kr
(J.-H.C., K.K., Y.S.G., C.S.C., S.G.S., H.-K.B., S.W.K., S.-J.C., S.R.L.)

Department of Geophysics
Kangwon National University
Chuncheon 24341, Republic of Korea
hoonyol@kangwon.ac.kr
(H.L.)

Mineral Resources Division
Korea Institute for Geosciences and Mineral Resources
Daejeon 34132, Republic of Korea
esbang@kigam.re.kr
(E.-S.B.)

Geoscience Platform Division
Korea Institute for Geosciences and Mineral Resources
Daejeon 34132, Republic of Korea
leehj@kigam.re.kr
gisyi@kigam.re.kr
(H.-J.L., S.S.L.)

Manuscript received 21 June 2018;
Published Online 12 February 2019